PAPER K

MIGRATION OF CROSSWELL SEISMIC DATA: SYNTHETIC ACOUSTIC CASE

Le-Wei Mo and Jerry M. Harris

ABSTRACT

This paper describes a complete acoustic P-wave modeling of the McElroy field data in Mo and Harris (1993b). It serves as a guide to processing field data.

It shows that direct wave must be removed before the data are input to migration processing, and this should be done not in the severe damage of reflections and diffractions. Vertical resolution of half wavelength can be achieved everywhere in the image plane. But horizontal resolution is slightly better at the side of the receiver well than at the source well.

INTRODUCTION

In a crosswell seismic survey geometry, the shots and receivers are located in separate wells. Thus crosswell migration is best considered as a problem of prestack common-shot profile migration. A profile consists of the seismograms of one shot and many receivers. Because it is a true physical experiment, processing of profiles is more fundamental than that of other geometries. Methods of prestack profile migration were first presented by Claerbout (1970, 1976). According to his *U/D* imaging concept, reflectors exist in the earth at places where the onset of the downgoing wave is time-coincident with an upcoming wave. Several authors have since extended Claerbout's theorem of wavefield extrapolation and the imaging condition (Reshef and Kosloff, 1986; Chang and McMechan, 1986). Chang and McMechan (1986) generalized Claerbout's imaging condition, and stated the excitation-time imaging condition for prestack reverse-time migration, by which each reflector point is imaged at the one-way direct-wave traveltime from the source to the point at which it is excited. Reverse-time profile migration with the excitation-time imaging condition consists of three elements: (1) computation of the imaging condition, that is, computation of the direct wave traveltime from the source point to every image point, (2) extrapolation backward in time of the common-shot profile wavefields from the receivers into the background velocity model by the two-way wave equation finite-difference method, and (3) imaging. Imaging is performed at each step of the wavefield extrapolation process by extracting, from the propagating wavefields, the values at the particular grid points that are excited and thus imaged at that time and adding them as reflectivity into the image plane at the same spatial locations. The locus of all points

imaged at one time step corresponds to the direct wave exciting wavefront from the source.

We have applied second-order-in-time, eighth-order-in-space staggered-grid finite difference method (Virieux, 1986; Dablain, 1986; Etgen, 1989) to solve the two-way acoustic wave equation for wave propagation. This numerical method warrants coarse grid calculation. Spatial sampling rate of about five points per wavelength is enough to avoid numerical dispersion, as oppose to sampling rate of fifteen points per wavelength that is required by second-order in time and space finite difference method (Alford et al., 1974). And computation is thus fast. And we have applied the finite difference method (Van Trier and Symes, 1990) to compute the direct wave traveltime used as the excitation time imaging condition for the prestack reverse time migration (Claerbout, 1985; Hu and McMechan, 1986).

THE INTERRELATION OF MODELING AND MIGRATION

To describe modeling, let us consider the 2-D geological model shown in Figure 1. It contains a point diffractor D in an arbitrary low-wavenumber velocity background. The recording geometry contains a source S located at one well and a series of receivers located at another well. During the modeling process, the direct wave emitted from the source S excites the diffractor D at a time equal to the minimum traveltime t_{SD} from the source S to the diffractor D, according to Fermat's principle. The diffractor D generates diffraction as rays DR that are recorded by the receivers. The diffraction wavefront expands from the diffractor. Modeling by the finite-difference method represents the wave equation by finite-differencing. The low-wavenumber velocity background and the high-wavenumber velocity heterogeneity are represented as attributes assigned to the finite-difference grids. Each grid point is treated as a point diffractor (or secondary source). The strength of each secondary source is proportional to the reflectivity at that location. The recorded data are the history wavefields at the recording grid points (Alford et al., 1974; McMechan 1985). During the process of modeling, the low-wavenumber velocity background governs the wave propagation, and the high-wavenumber velocity heterogeneity generates the diffractions. Crosswell seismic survey is usually conducted at a subsurface segment of the well that covers the target zone; thus, during the numerical modeling process, the absorbing boundary conditions of Cerjan et al (1985) are applied along the four sides of the grid to simulate a whole space for wave propagation.

Transmission traveltime tomography recovers the low-wavenumber smooth background velocity by using the direct wave traveltimes. Migration is the process that backprojects the recorded diffraction wavefields from the recording boundary into the low-wavenumber velocity background to locate the diffractors, which constitutes of the high-wavenumber velocity heterogeneity. And if the direct wave is included in the migration process, it would image the original source. What is needed as additional input is a low-wavenumber velocity background model that governs the wave propagation. Migration produces the image of high-wavenumber velocity heterogeneity,

that is, the locations and strengths of the diffractors. Reverse-time depth migration projects the recorded diffraction wavefields back into the low-wavenumber velocity background by taking the recorded data as boundary values of a finite-difference grid and running backward through time (McMechan, 1983). The diffraction wavefront focuses toward the location of the original diffractor. At time t_{SD}, all the energy that was diffracted at D will be focused at D. The value of the backpropagating wavefields at the particular grid point of D is extracted and then added as reflectivity into the image plane at the same spatial location (Chang and McMechan, 1986). As the wavefields continue to propagate backward in time, the focused energy at D defocuses and continues to backpropagate in the way each contribution originates. Each grid point is treated as a point diffractor and is imaged accordingly.

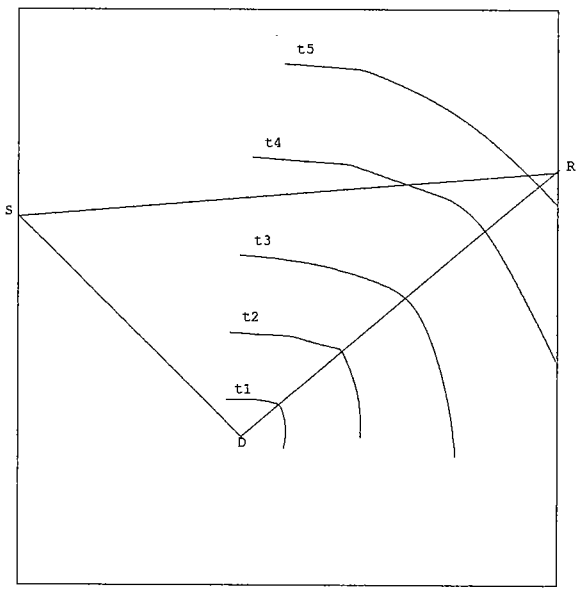

Figure 1: During modeling, the secondary diffraction wavefront expands from diffractor D. During reverse-time migration, the diffraction wavefront focuses toward diffractor D.

SYNTHETIC MODEL BUILDING

There are two kinds of reflectors, namely boundary reflectors and scattering reflectors. Boundary reflectors are those reflectors between two different rock blocks, whose thicknesses are larger than a wavelength. Scattering reflectors are those reflectors corresponding to local heterogeneities, whose thickness is smaller than a wavelength, such as the fault plane zone. Reflections from opposite sides of a boundary reflector have opposite polarities. Reflections from opposite sides of a scattering reflector have the same polarity. Thus in the crosswell survey, stacking or subtracting the reflection images corresponding to upgoing incidence and downgoing incidence waves would result in enhancement or cancellation of one of the two kinds of reflections. In the viewpoint of which velocity is composed of low- and high- wavenumber bands and from the experience we observe sonic logs and field geology, we believe that scattering reflectors are more common than boundary reflectors. In this paper, we demonstrate

scattering reflectors. Demonstration of boundary reflectors will be presented in future publications.

Figure 2 shows a vertically and horizontally variable but smooth background velocity model, whose velocity ranges from 15000 ft/s to 21000 ft/s. The grid size is 480 x 148. This model is derived from the result of transmission traveltime tomography (Van Schaack et al, 1992) after some smoothing to attenuate the effects of possible artifacts in the tomogram. The portion above 2650 ft and the portion below 3150 ft are made by extrapolating the original tomogram velocity model. The two wells are separated by 184 ft. We made the final velocity model by superimposing high-wavenumber velocity contrast heterogeneities (either low or high velocity layer, whose thickness is less than a wavelength, say, one grid point in a finite difference grid) in the above smooth background velocity model. Figure 3 shows the geometry of the scattering reflectors. The dimension of the vertical splitting in the reflectors at depth of 2625 ft, 2700 ft and 2900 ft is 8 ft, that is, half wavelength. The dimension of the horizontal holes in the reflectors at depth of 2800 ft, 2850 ft, 3100 ft and 3175 ft is 30 ft, that is, one-and-half wavelengths. The dip of the reflectors at depth of 2650 ft and 3150 ft is 10 degrees. The dip of the reflectors at depth of 3000 ft is 15 degrees. These velocity contrast heterogeneities generate reflections and diffractions during forward modeling.

SYNTHETIC MODELING

The crosswell survey is conducted in a segment of the wells. The wavelet used in the finite-difference modeling is the first derivative of the Gaussian function (Alford et al, 1974), the frequency ranges from 200 Hz to 2500 Hz, with the fundamental frequency being 1000 Hz. The dominant wavelength is 18 ft; the smallest wavelength is 6 ft. The horizontal and vertical grid spacing is 1.25 ft. Thus the spatial sampling is 5 points per wavelength for the smallest wavelength, which is a coarse sampling interval. If second-order-in-space central finite-differences were used, this spatial sampling would create severe grid dispersion. For the second-order-in-time, eighth-order-in-space staggered-grid finite differencing scheme employed in this paper, the numerical accuracy is good.

PRESTACK REVERSE-TIME MIGRATION

As we pointed out above that if the direct wave is included in the migration process, it would image the original source. We show the effects of muting and not muting the direct waves before migration. We arrive at the conclusion that direct wave must be removed before the data are input to migration processing.

Not muting the direct wave

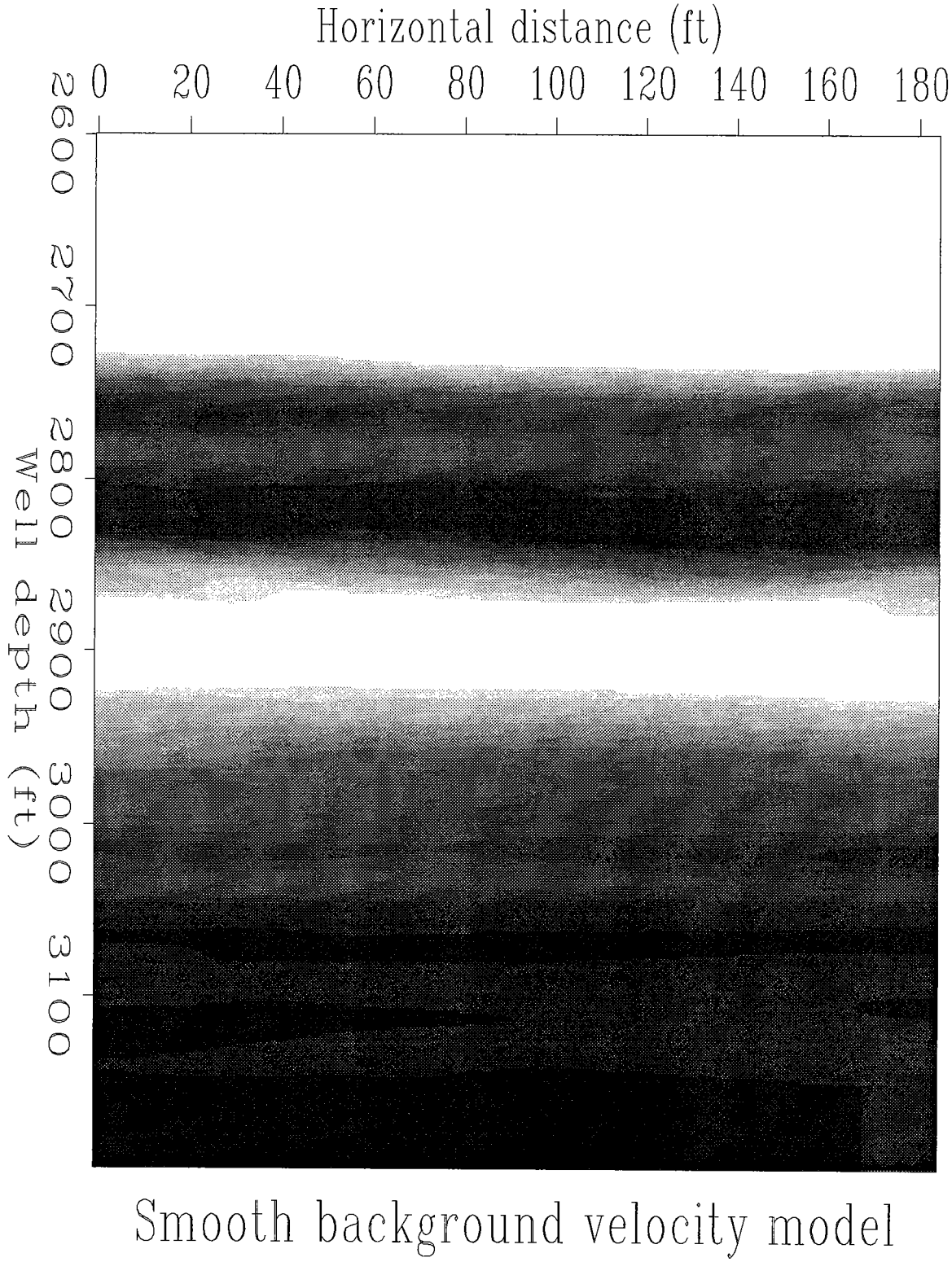

Figure 2: A smooth background velocity model, in which high-wavenumber velocity heterogeneity reflectors will be superimposed. White (black) means low (high) velocity.

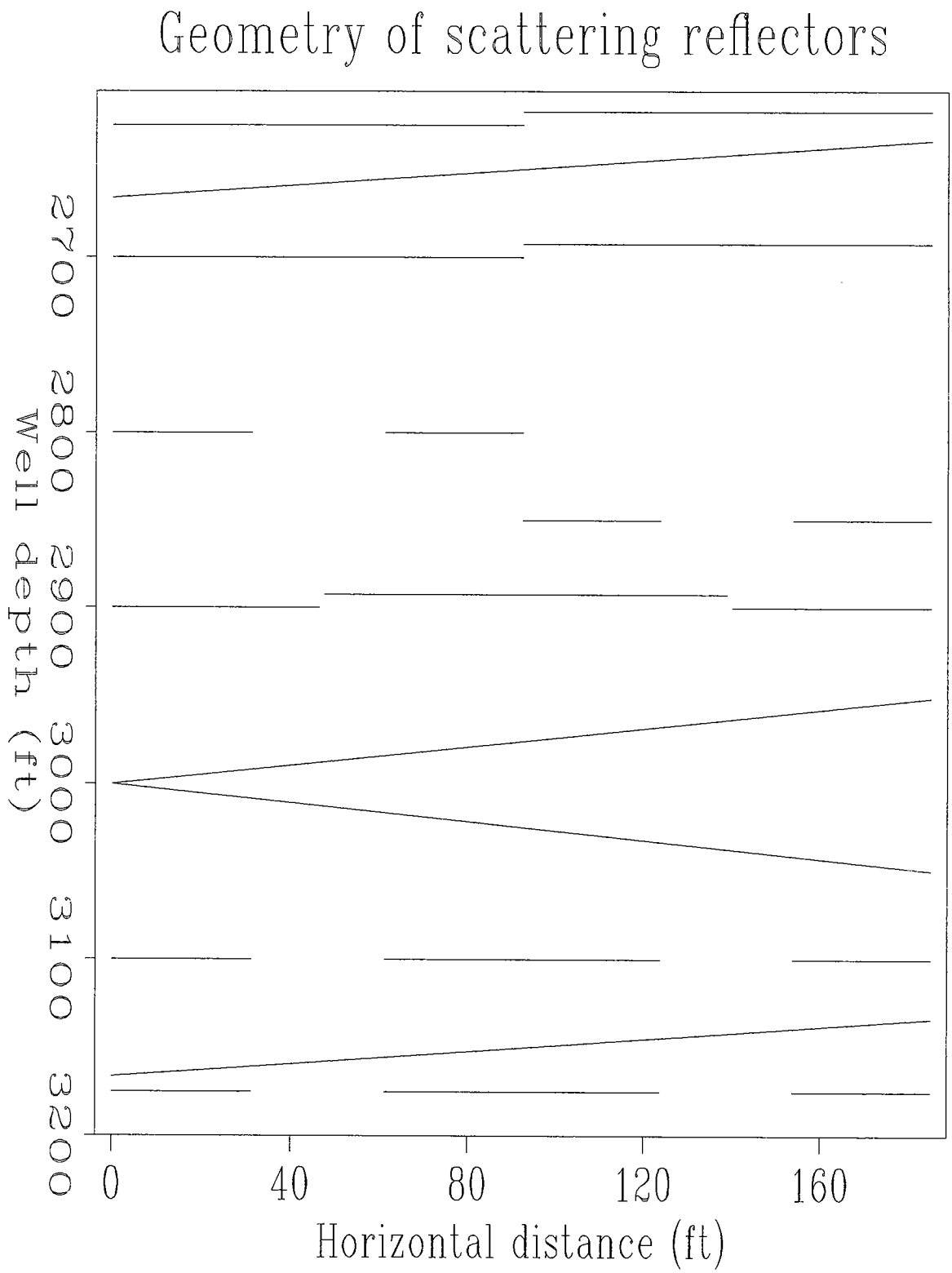

Figure 3: Scattering reflectors to be superimposed in the smooth background velocity model of Figure 2.

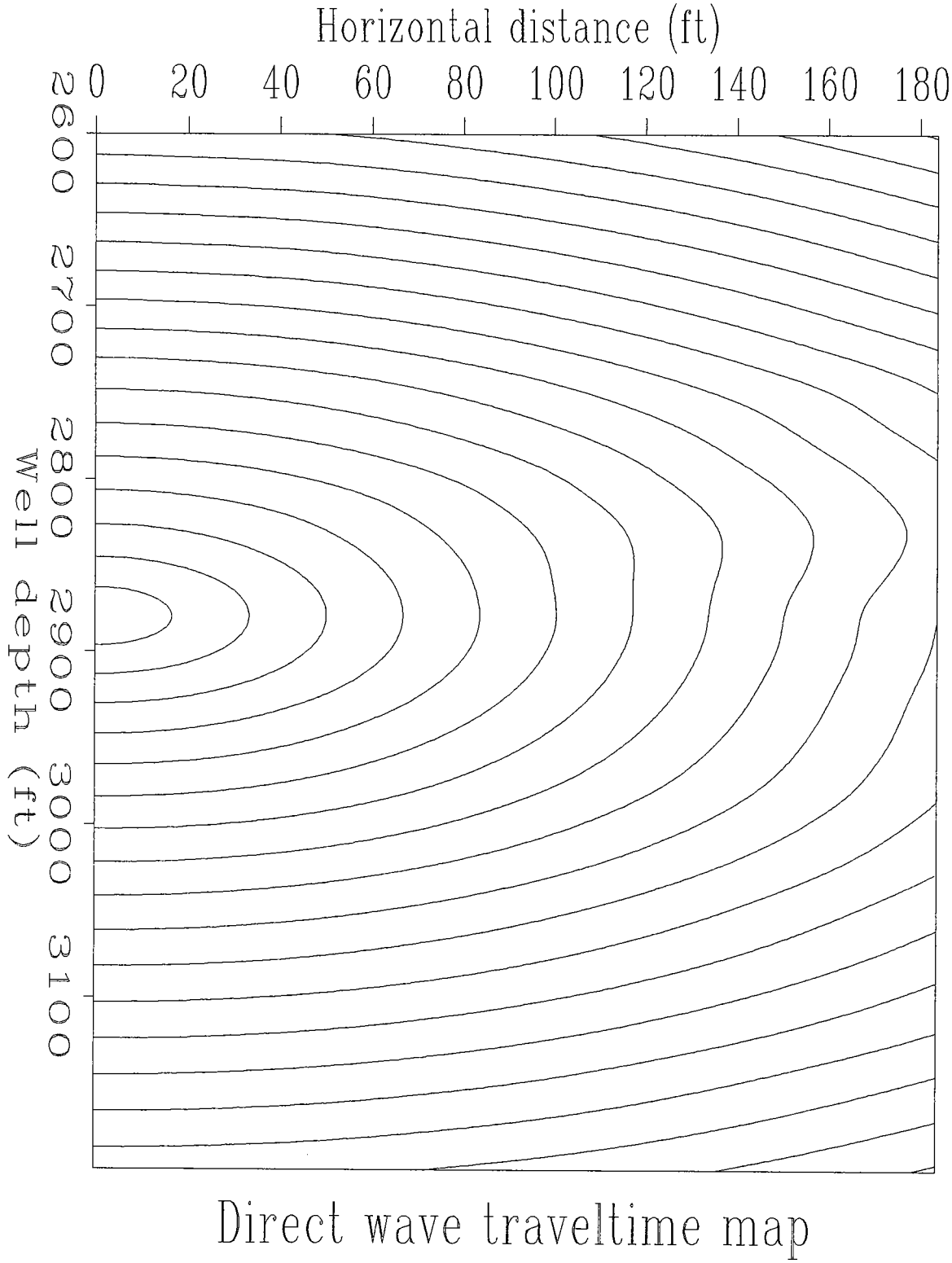

Figure 4: Contour of the direct wave traveltime from the source at depth of 2880 ft in the left well.

Figure 5 is the synthetic common-shot profile data with the source located at depth of 2880 ft in the left well and the receivers equally spaced at a depth interval of 1.25 ft in the right well from depth of 2650 ft to 3150 ft.

Figure 4 shows the direct-wave traveltime contour map from the source computed by finite-difference method (Van Trier and Symes, 1990). It shows the time that a diffractor is excited during modeling and also the time that the diffractor is imaged during migration wavefield backpropagation. With the recorded common-shot profile data as boundary conditions along the recording grid points, we run the two-way wave equation backward in time. Imaging is performed at each step of the wavefield extrapolation by extracting the values of the grid points that are imaged at that time as reflectivity and putting them into the image plane at the same locations. The locus of all points that are imaged at a particular time step corresponds to the direct wave exciting wavefront from the source. The common-shot profile data that are input for migration processing are without divergence corrections because of the reversibility of modeling-migration conjugacy, which is explained in Appendix A. Figure 6 shows the reflectivity depth image between the two wells produced by migrating the data of Figure 5. Notice that the original source is imaged, and at the same time there are also some artifacts owing to the inclusion of the direct wave in the migration process. Notice that the image of the original source is sharp, and the artifacts are generally smooth, and their dips are variant. Thus they can not be effectively removed by wavenumber filtering or 2-D dip filtering. It shows that **the direct wave must be removed before migration.** And this should be done not in the severe damage of the reflections and diffractions because they overlay to some extent.

Muting direct wave

Figure 7 is the same synthetic common shot gather as that of Figure 5, but the direct wave has been muted. Figure 8 is the corresponding migration image. Because of the removal of the effects of the direct wave, this image is better than that of Figure 6. Depending on the source and reflector orientation, some of the reflectors have been correctly recovered. We made 178 common shot gather modelings and migrations, the same size as the McElroy field data. The shots are evenly spaced at an interval of 2.5 ft from depth of 2687.5 ft to 3130 ft in the left well. And the receivers are evenly spaced at an interval of 1.25 ft from depth of 2650 ft to 3150 ft in the right well. Figure 9 is the stacked image. Comparing this stacked image to the reflector model of Figure 3 shows that all the reflectors have been correctly imaged. And the background of the image is clean.

The portion of the image above 2650 ft and that below 3150 ft are out of the range of the receivers, showing the ability of the algorithm to image those reflectors out side of the survey area. And the vertical and horizontal resolutions remain the same.

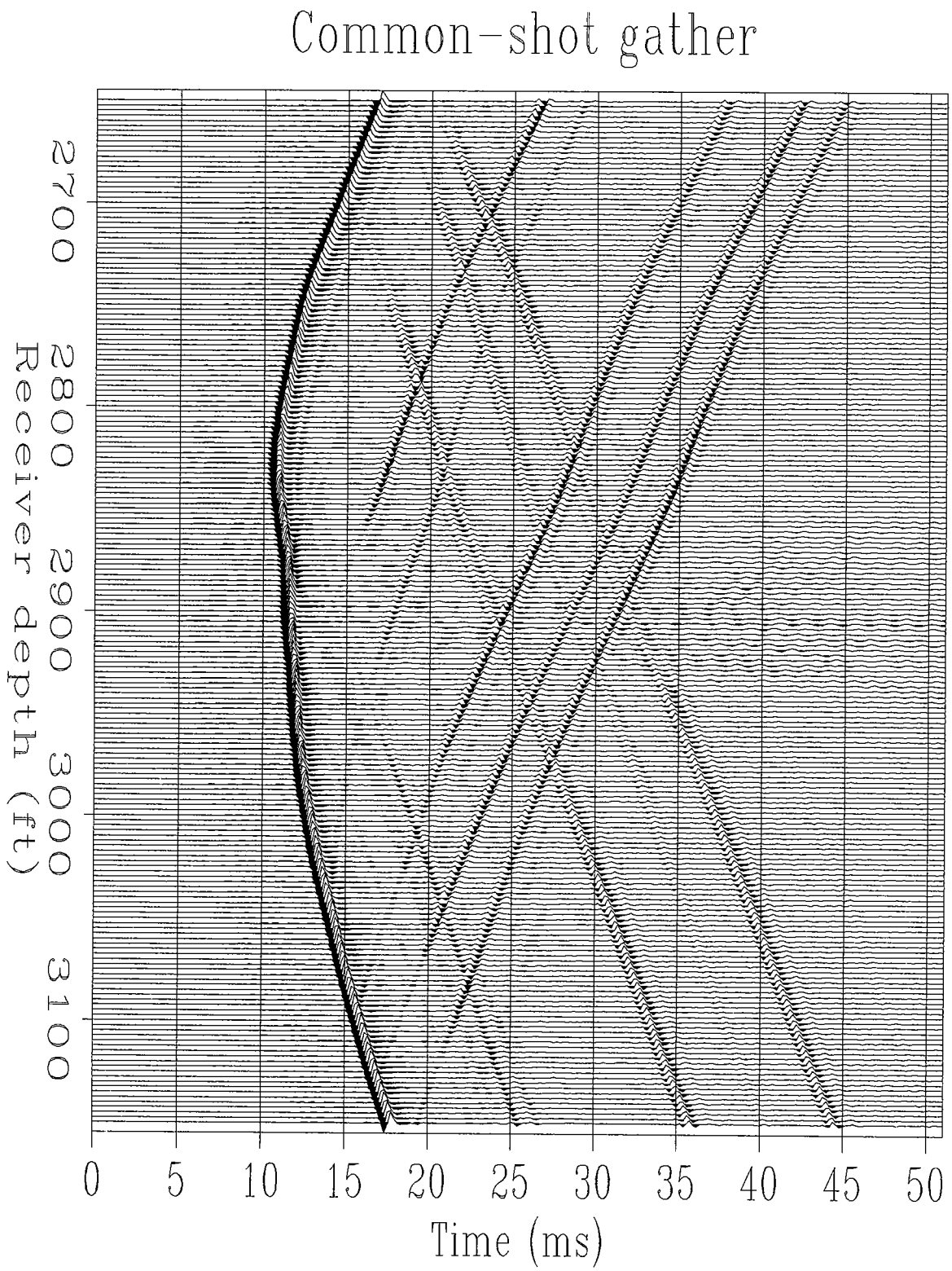

Figure 5: A synthetic common shot gather. The shot is located at a depth of 2880 ft in the left well. This data has been gained by AGC.

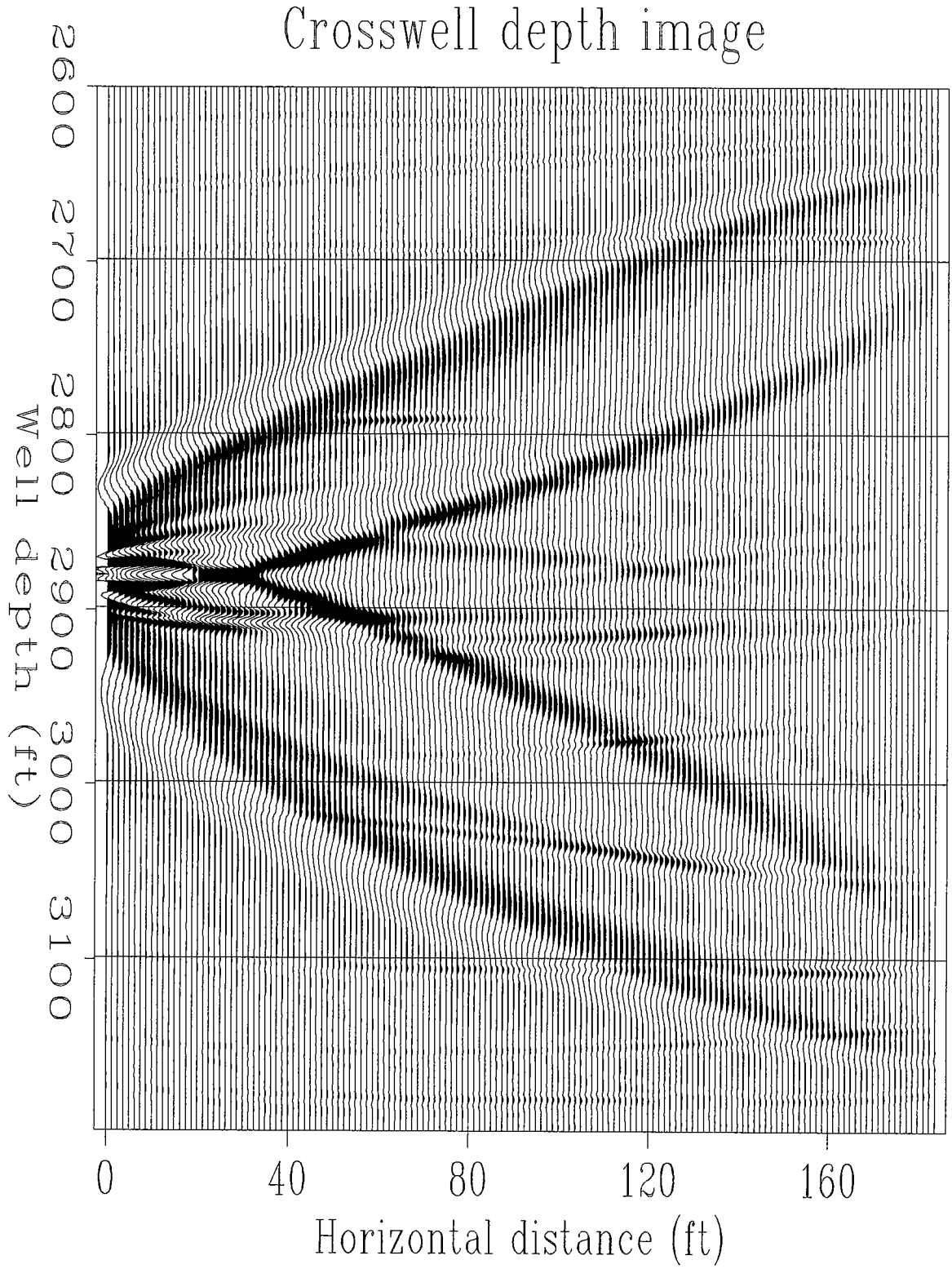

Figure 6: The image produced by migrating the common shot gather of Figure 5.

It shows that vertical resolution of half wavelength can be achieved everywhere in the image plane. But horizontal resolution is slightly better at the side of the receiver well than at the source well.

Notice that the complicated reflectors generate complex reflections in the data of common shot gather. There are horizontal holes in the reflectors in Figure 3, but the reflection events are all continuous owing to diffraction. Diffraction events can be seen on the common shot gather data of Figure 5 and Figure 7. And there are not much differences between the reflection events of horizontal and dipping reflectors. If VSP-CDP mapping (Stewart and Marchisio, 1991; Lazaratos, 1993) were used to process this data, it would produce incorrect results. Because of the inherent assumption of 1-D geology in VSP-CDP mapping, it would not image the dipping reflectors correctly. And for the horizontal reflectors with holes on them, VSP-CDP mapping would image them as continuous reflectors, because ray-theoretic VSP-CDP mapping does not focus diffraction energy, and thus does not collapse Fresnel zone.

CONCLUSIONS

Acoustic crosswell seismic modeling and migration have been successfully performed for a true field survey geometry by using high-order finite differencing. Direct wave must be removed before the data are input to migration processing, and this should be done not in the severe damage of reflections and diffractions. Vertical resolution of half wavelength can be achieved everywhere in the image plane. But horizontal resolution is slightly better at the side of the receiver well than at the source well.

ACKOWLEDGEMENTS

Our thanks to Prof. Jon Claerbout of Stanford Exploration Project, Prof. Andre Journel of Stanford Center for Reservoir Forecasting for allowing us to use their computers. We are grateful to Jos van Trier for sharing with us his codes of finite difference traveltime calculation, and to John Etgen for sharing with us his codes of finite difference wave equation solver.

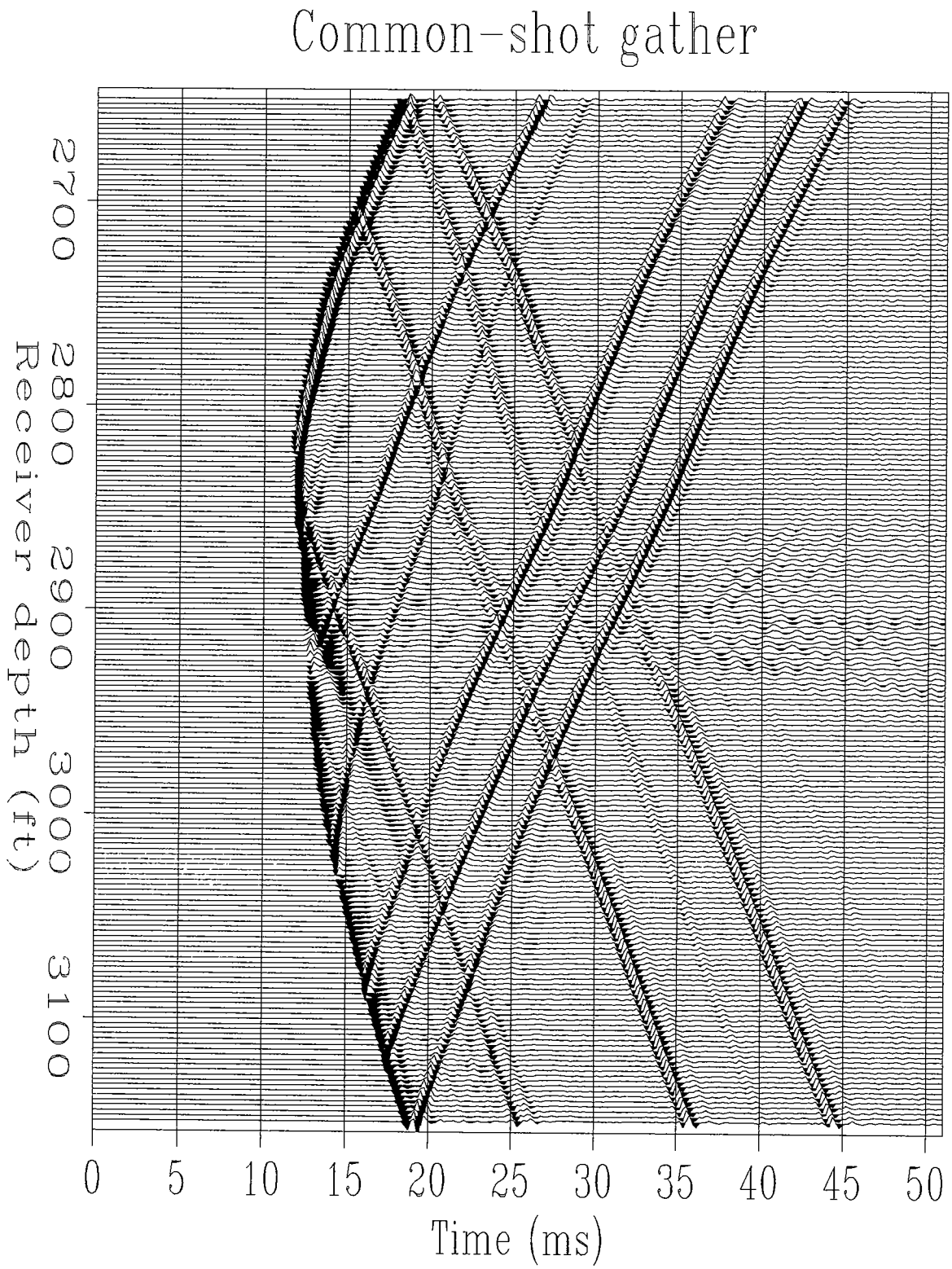

Figure 7: The same synthetic common shot gather as that of Figure 5, but the direct wave has been muted. This data has been gained by AGC.

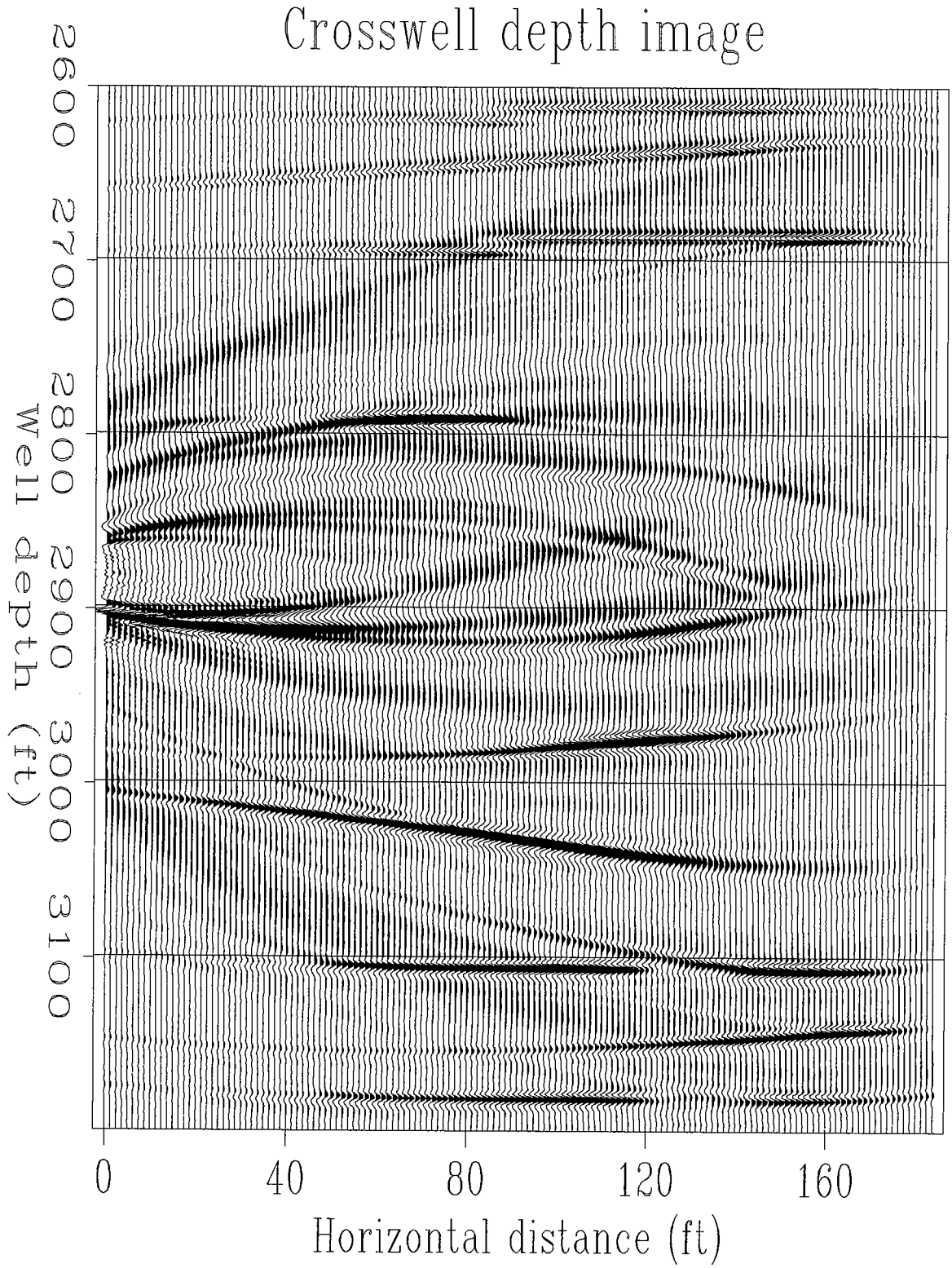

Figure 8: The image produced by migrating the common shot gather of Figure 7.

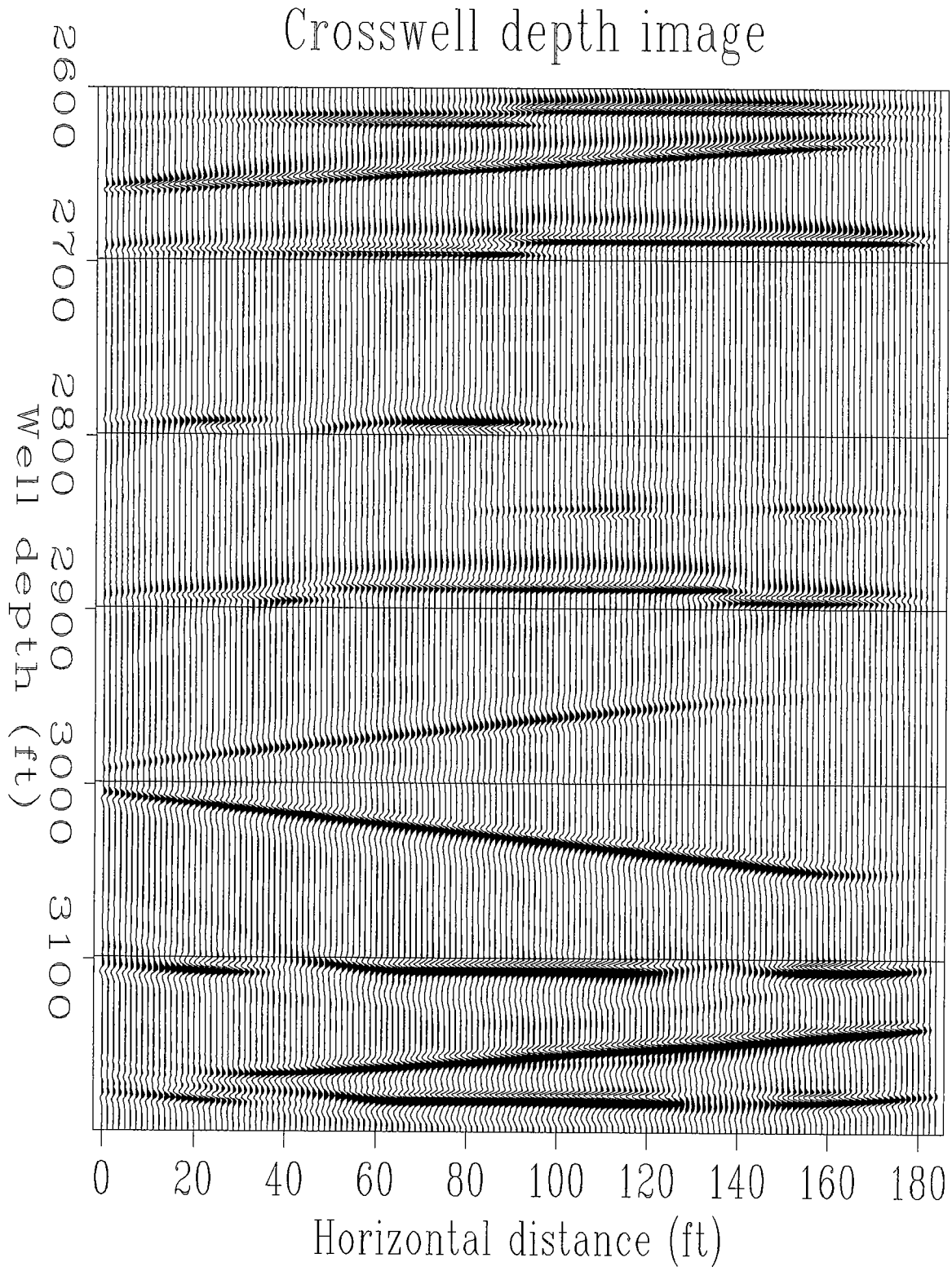

Figure 9: The image produced by stacking 178 individual images like that of Figure 8

REFERENCES

Alford, R. M., Kelly, K. R., and Boore, D. M., 1974, Accuracy of finite-difference modeling of the acoustic wave equation: Geophysics, **39**, 834–842.

Cerjan, C., Kosloff, D., Kosloff, R., and Reshef, M., 1985, A nonreflecting boundary condition for discrete acoustic and elastic wave equations: Geophysics, **50**, 705–708.

Chang, W. F., and McMechan, G. A., 1986, Reverse-time migration of offset vertical seismic profiling data using the excitation-time imaging condition: Geophysics, **51**, 67–84.

Claerbout, J. F., 1970, Coarse grid calculations of waves in inhomogeneous media with application to delineation of complicated seismic structure: Geophysics, **35**, 407–418.

Claerbout, J. F., 1976, Fundamentals of Geophysical Data Processing: McGraw-Hill.

Claerbout, J. F., 1985, Imaging the Earth's Interior: Blackwell Scientific.

Claerbout, J. F., 1991, Earth Soundings Analysis: Processing versus Inversion: Blackwell Scientific.

Dablain, M., 1986, The application of high-order differencing to the scalar wave equation: Geophysics, **51**, 54–66.

Etgen, J., 1989, Accurate wave equation modeling: SEP–**60**, 131–148.

Gray, S., and Lines, L., 1992, Cross-borehole tomographic migration: Amoco Research Center.

Hu, L. Z., McMechan, G. A., and Harris, J. M., 1988, Acoustic pre-stack migration of cross-hole data: Geophysics, **53**, 1015–1023.

McMechan, G. A., 1983, Migration by extrapolation of time-dependent boundary values: Geophys. Prosp., **31**, 413–420.

McMechan, G. A., 1985, Synthetic finite-offset vertical seismic profiles for laterally varying media: Geophysics, **50**, 627–636.

Mo, L., and Harris, J. M., 1993b, Migration of crosswell seismic data: Field data case: STP–**4**, paper-L.

Reshef, M., and Kosloff, D., 1986, Migration of common-shot gathers: Geophysics, **51**, 324–331.

Van Schaack, M., 1992, High resolution crosswell imaging of a West Texas Carbonate reservoir: Part 3 – traveltime tomography: STP–**3**, paper-C.

Van Trier, J., and Symes, W. W., 1990, Upwind finite-difference calculation of traveltimes: SEP–**65**, 41–58.

Virieux, J., 1986, P-SV wave propagation in heterogeneous media: Velocity-stress finite-difference method: Geophysics, **51**, 889–901.

APPENDIX

The input to prestack reverse-time migration

Prestack reverse-time migration is the process that transfers recorded scattered data into the subsurface image through the two-way wave equation. The wave equation can be made to run both forward and backward in time. When the wave equation runs forward in time, it is a modeling process that transfers the subsurface reflectivity into scattered fields. When the wave equation runs backward in time, it is a migration imaging process that transfers the recorded scattered wavefields into the subsurface reflectivity image. The two processes are conjugate to each other (Claerbout, 1991), because the wave propagation wavefront is reversible. Thus the input to reverse-time migration is the recorded scattered data without divergence correction.